



Engineered bovine serum albumin-based nanoparticles with pH-sensitivity for doxorubicin delivery and controlled release

Zhihang Yang , Na Zhang , Teng Ma , Libo Liu , Lini Zhao & Hui Xie

To cite this article: Zhihang Yang , Na Zhang , Teng Ma , Libo Liu , Lini Zhao & Hui Xie (2020) Engineered bovine serum albumin-based nanoparticles with pH-sensitivity for doxorubicin delivery and controlled release, Drug Delivery, 27:1, 1156-1164, DOI: [10.1080/10717544.2020.1797243](https://doi.org/10.1080/10717544.2020.1797243)

To link to this article: <https://doi.org/10.1080/10717544.2020.1797243>



© 2020 The Author(s). Published by Informa UK Limited, trading as Taylor & Francis Group.



[View supplementary material](#)



Published online: 05 Aug 2020.



[Submit your article to this journal](#)



Article views: 222



[View related articles](#)



[View Crossmark data](#)

Engineered bovine serum albumin-based nanoparticles with pH-sensitivity for doxorubicin delivery and controlled release

Zhihang Yang^a, Na Zhang^b, Teng Ma^{c,d}, Libo Liu^{c,d}, Lini Zhao^e and Hui Xie^f

^aDepartment of Physiology, College of Basic Medicine, Shenyang Medical College, Shenyang, China; ^bDepartment of Electrical Diagnosis, Central Hospital Affiliated to Shenyang Medical College, Shenyang, China; ^cDepartment of Neurobiology, School of Life Sciences, China Medical University, Shenyang, China; ^dKey Laboratory of Cell Biology, Ministry of Public Health of China, and Key Laboratory of Medical Cell Biology, Ministry of Education of China, China Medical University, Shenyang, China; ^eDepartment of Pharmacology, College of Basic Medicine, Shenyang Medical College, Shenyang, China; ^fDepartment of Histology and Embryology, College of Basic Medicine, Shenyang Medical College, Shenyang, China

ABSTRACT

In this work, we prepared a stimuli-responsive system for drug delivery and controlled release by engineering the bovine serum albumin (BSA). The doxorubicin (DOX)-loaded BSA nanoparticles (NPs) were conveniently prepared using desolvation method, followed by crosslinking through Schiff base bonds, leading to pH-sensitive DOX-loaded system (DOX_s@BSA NPs). The resulted DOX_s@BSA NPs showed high drug loading capacity (21.4%), and the particle size was about 130 nm with narrow polydispersity and high negative surface charge (−20.5 mV). The pH-sensitivity of DOX_s@BSA NPs was evidenced by the size changes and charge reversal after incubation at different pH values. The DOX_s@BSA NPs showed high serum stability which indicated the prolonged circulation time. The *in vitro* drug release experiment showed that the release of DOX was obviously accelerated by acidity because of disassembly of NPs induced by cleavage of Schiff base bonds. The drug release mechanism was thoroughly studied using a semi-empirical model, further confirming the pH played an important role in drug controlled release process. The results of cytotoxicity assay revealed that DOX_s@BSA NPs exhibited much higher toxic effects for tumor cells in comparison to the free DOX control. Collectively, these results demonstrated that DOX_s@BSA NPs might be potential application for drug delivery and controlled release in cancer chemotherapy. Moreover, this work also showed that preparation of stimuli-responsive drug delivery system by engineering the commercial biomaterials could be a promising method to develop multi-functional nanomedicine.

ARTICLE HISTORY

Received 28 May 2020
Revised 7 July 2020
Accepted 13 July 2020



KEYWORDS

BSA; pH-sensitivity; drug delivery; controlled release; cancer therapy

1. Introduction

Cancer has become the leading killer of humans, causing 9.6 million of death and US\$1.16 trillion of economic cost every year (Copur 2019; Datta et al. 2019; Ferlay et al. 2019). With the rapid development of nanotechnology and material engineering, some emerging therapies including photothermal therapy (PTT), photodynamic therapy (PDT), gene therapy and immunotherapy, have been developed in these years (Mellman et al. 2011; Zhang et al. 2017; Zeng et al. 2019; Riley et al. 2019; Xu et al. 2020). However, the therapeutic efficacy and biosafety have to be further improved and evaluated before clinic use (Yang et al. 2013; Dickmann et al. 2014; Fakhoury 2016). So far, traditional chemotherapy is still the most common and useful approach to treat the cancer clinically. In these decades, many chemical anticancer drugs have been synthesized and prepared, such as doxorubicin (DOX), paclitaxel (PTX), and camptothecin (CPT), for cancer chemotherapy (Gordon et al. 1995; Lai et al. 2007;

Min et al. 2008; Oh et al. 2010). However, the small molecular drugs have their own limitations in clinical applications, such as quick clearance by reticuloendothelial system (RES), low anticancer efficacy and severe side-effect (Brannon-Peppas and Blanchette 2004; Guo and Huang 2011; Sandhu et al. 2015). For example, DOX which can interact with DNA by intercalation and inhibition of macromolecular biosynthesis is one of the most effective drugs for a wide range of cancers including breast cancer, bladder cancer, lymphoma, and acute lymphocytic leukemia (Soma et al. 2000; Sharma 2017; Sun et al. 2019; Zhou et al. 2020). Even though DOX was approved for medical use in the United States 45 years ago (Agarwal et al. 2011), the side-effects severely limit the wide use in clinic, such as hair loss, bone marrow suppression, vomiting, rash, and inflammation of the mouth, especially the dilated cardiomyopathy which can lead to congestive heart failure (Singal and Iliskovic 1998; Chatterjee et al. 2010; Dong et al. 2017). To overcome these obstacles, drug delivery system (DDS) has been thoroughly investigated and

CONTACT Zhihang Yang  yzhsmc@sina.com 

 Supplemental data for this article can be accessed [here](#).

© 2020 The Author(s). Published by Informa UK Limited, trading as Taylor & Francis Group.

This is an Open Access article distributed under the terms of the Creative Commons Attribution License (<http://creativecommons.org/licenses/by/4.0/>), which permits unrestricted use, distribution, and reproduction in any medium, provided the original work is properly cited.

extensively used to develop nano-scale formulations for improving the therapeutic efficacy and reducing the side-effects, especially the stimuli-responsive biomaterials-based DDSs (Gong et al. 2012; Mura et al. 2013; Yin et al. 2013; Li et al. 2014; Sun et al. 2014; Masood 2016; Qiao et al. 2019). Considering the specific tumor microenvironments such as low pH (Zhang et al. 2019), high glutathione (GSH) concentration and special enzyme (Kong et al. 2016; Li et al. 2019), various stimuli-responsive biomaterials including biopolymer (Li et al. 2018), inorganic nanoparticles (Baeza et al. 2015), and metal-organic frameworks have been developed and used as chemical anticancer drug carriers to improve the cancer chemotherapy (Chen et al. 2018; Wang et al. 2020). However, before these multi-functional nanocarriers can be considered for clinical applicability, two vital challenges have to be addressed. One is the synthesis of these biomaterials should need to be adapted for scaling-up, so as to minimize polydispersity in size and surface chemistry. The other one is the biosafety including cytotoxicity, biocompatibility and biodegradation which have to be further evaluated. Conversely, some traditional and commercial biomaterials-based NPs (e.g. poly(lactic acid) (PLA), poly lactic-co-glycolic acid (PLGA)) used as drug delivery systems do not exhibit multi-functionality, such as pH-triggered drug release behavior, charge reversal, improved cellular uptake (Byrne and Deasy 2002; Makadia and Siegel 2011; Larrañeta et al. 2016; Saini et al. 2016). Particularly, although the commercial BSA shows non-toxic effect and high biosafety (Mariam et al. 2016; Saha et al. 2019), BSA does not have the stimuli-responsiveness for controlled release of encapsulated cargos. It's of great interest and significance to develop functional drug delivery system based on BSA with high drug loading capacity and stimuli-responsive property.

In this work, we designed and developed an engineered BSA-based NP for delivery of DOX with pH-triggered release profile. Anticancer drug DOX is physically loaded into the BSA-based NPs using desolvation method, resulting in DOX-loaded BSA NPs (named after DOX@BSA NPs). And then, glutaraldehyde is used to crosslink the BSA through the interaction between aldehyde and amine residues, resulting in Schiff base bond which is pH-sensitive (named after DOX_s@BSA NPs) (Feng et al. 2017; Peng et al. 2019; Xu et al. 2019). The physicochemical properties of DOX_s@BSA NPs including particle size, zeta-potential, serum stability, drug release behavior and mechanism, and cytotoxicity were investigated by a variety of experimental techniques.

2. Materials & methods

2.1. Materials

Doxorubicin hydrochloride (DOX-HCl) was purchased from Wuhan Yuan Cheng Gong Chuang Co. Bovine serum albumin (BSA, ≥98%), glutaric acid (≥99%), glutaraldehyde, triethylamine (TEA, ≥99%) and methylthiazoltetrazolium (MTT) were purchased from Sigma (St. Louis, MO). Dulbecco's modified eagle media (DMEM) growth media, fetal bovine serum (FBS), trypsin, penicillin and streptomycin, were all purchased from Invitrogen; NIH 3T3, A549, A2780 and NCL-H460 cell lines

were obtained from the American Type Culture Collection (ATCC). All other reagents were used as received.

2.2. Preparation of DOX_s@BSA NPs

BSA NPs were prepared by the desolvation technique (Chen et al. 2014; Chu et al. 2015). Briefly, BSA was first dissolved in deionized water at the concentration of 20 mg/mL with stirring at room temperature. The dimethyl sulfoxide (DMSO) was then added into the BSA solution (1: 5, v/v) with stirring. Thirty minutes later, ethanol was quickly added into the BSA solution (3.5: 1, v/v) under low stirring at room temperature. The reaction was carried on for 2 h. To prepare the stable and pH-responsive BSA NPs, glutaraldehyde (2%, 120 μL per 1 mL BSA solution) was added, and the reaction was carried on for 24 h. After that, the resulted solution was centrifuged at 20,000 g for 30 min at 4 °C. The received pellets were re-suspended in deionized water, and centrifuged again. This step was repeated three times to remove organic solvents. The obtained crosslinked BSA NPs (sBSA NPs) was re-suspended in phosphate buffer solution (PBS, pH 7.4) for the follow-up experiments. Furthermore, glutaric acid was used to replace the glutaraldehyde to prepare pH-insensitive BSA NPs (iBSA NPs) which was used as negative control in future.

To prepare the pH-responsive DOX-loaded BSA NPs (DOX_s@BSA NPs), the DOX-HCl (5 mg, 10 mg, 20 mg) was dissolved into DMSO, and then the TEA (0.1 μL of TEA per 1 mg of DOX) was added with stirring. The mixed solution was stirred at least for 30 min in dark at room temperature. BSA solution (1 mL, 20 mg/mL) was added and incubated for 15 min. The followed steps were similar. After desolvation and crosslink, the obtained solution was centrifuged (20 000 rpm, 30 min) to remove the organic solvents and the unencapsulated drugs. After that, the DOX_s@BSA NPs were obtained and kept in 4 °C for use in future.

2.3. Characterization of DOX_s@BSA NPs

The particle size, size distribution (polydispersity index, PDI) and zeta-potential of iBSA NPs, sBSA NPs and DOX_s@BSA NPs were measured by dynamic light scattering (DLS, Malvern Zetasizer Nano S, Malvern, UK).

To evaluate the stability of DOX_s@BSA NPs, 1 mL of DOX_s@BSA NPs (1 mg/mL) was re-suspended into 1 mL of PBS at pH 7.4 with 20% FBS, followed by incubation for different time at 37 °C. The particle size of sample was recorded every day. Furthermore, DOX_s@BSA NPs were re-suspended into PBS (pH 7.4) or 5% glucose at the concentration of 1 mg/mL. And then, the solution was diluted at 1/1, 1/10, 1/100 and 1/1000 of original concentration. The particle size of sample was then measured using DLS.

To study the pH-sensitivity, the particle size and zeta-potential of iBSA NPs, sBSA NPs and DOX_s@BSA NPs in PBS at different pH values were measured. In brief, the NPs were re-suspended into PBS with different pH values (3.0, 4.0, 5.0, 5.5, 6.5, 7.4 and 8.0) at the concentration of 1 mg/mL, followed by incubation for 24 h at 37 °C. And then, the samples were measured using DLS aforementioned.

2.4. Drug loading capacity

UV-vis spectrophotometer (UV-2450, Shimadzu, Japan) was used to confirm the drug loading content (LC) and encapsulated efficiency (EE) of DOX_s@BSA NPs. Briefly, 1 mL of supernate after centrifugation was measured using UV-vis spectrophotometer at 480 nm to confirm the concentration of DOX. And then, the amount of unloaded DOX was calculated according to the standards curve. The LC was defined as mass ratio of (DOX in feed-unloaded DOX) to DOX_s@BSA NPs. The EE was defined as mass ratio of (DOX in feed-unloaded DOX) to DOX in feed.

2.5. In vitro DOX release from DOX_s@BSA NPs

The *in vitro* DOX release profile from DOX_s@BSA NPs was studied using dialysis method. This experiment was performed at a quite low drug concentration to mimic the sink condition (Zhang et al. 2012). In brief, 4 mg of DOX_s@BSA NPs was re-suspended into 4 mL of PBS at pH 7.4, 6.5 and 5.0, and transferred into a dialysis bag (molecule weight cut-off, MWCO, 3500 Da). This dialysis bag was immersed into the corresponding PBS (46 mL, pH 7.4, 6.5 or 5.0) in a beaker at 37 °C with stirring at 110 rpm. At predetermined time interval, 1 mL of solution in the beaker was taken out for UV-vis analysis, and 1 mL fresh PBS was added. The free DOX was used as control. The cumulative drug release percent (E_t) was calculated according to the following equation:

$$E_t(\%) = \frac{V_e \sum_{i=1}^{n-1} C_i + V_0 C_n}{m_{\text{DOX}}} \times 100\%$$

where, m_{DOX} was the loaded DOX in BSA NPs, V_e and V_0 were, respectively, the volume of buffer in dialysis bag (4 mL) and the total volume of buffer (50 mL), and C_i was the DOX concentration in the i_{th} sample.

2.6. Cell culture

The NIH 3T3, A549, A2780 and NCL-H460 cell lines were cultured according to the standard protocol from supplier with a few modifications. In brief, the cells were cultured in fresh DMEM containing 10% (v/v) FBS, 100 units/mL penicillin, and 100 µg/mL streptomycin in a flask, and incubated at 37 °C in a CO₂ (5%) incubator. The cells were checked every day, and approximately separated every 2 or 3 days.

2.7. Cytotoxicity test

The cytotoxicity of BSA NPs, free DOX and DOX_s@BSA NPs against NIH 3T3, A549, A2780 and NCL-H460 cells were investigated by the standard MTT assay (Wei et al. 2017). As a typical experiment, cells were seeded into 96-cell plate at density of 1×10^4 cells per well in 200 µL of DMEM. The plate was incubated for 24 h. After that, the medium was removed, and pre-prepared samples in DMEM were added into the well. For BSA/DMEM solution, the series of concentrations were 5.0, 10, 100, 200, 300 and 400 µg/mL. For free

DOX/DMEM and DOX_s@BSA NPs/DMEM, the concentrations of DOX were 0.1, 0.5, 1.0, 2.0, 5.0, 10 and 20 µg/mL. Pure DMEM was used as background, and cell with medium was used as control. After 48 h incubation, the medium was removed and the well was washed three times using PBS. 100 µL of MTT solution (1 mg/mL in DMEM) was added into each well. And the plate was further incubated for 4 h. And then, the solution was removed, and 100 µL of DMSO was added to dissolve the crystal. After shaking for 15 min, the plate was measured at by a microplate reader (Multiskan Spectrum, Thermo Scientific, Finland) at 570 nm. The cell viability was calculated using the following equation:

$$\text{Cell viability} = \frac{A_{\text{sample}} - A_{\text{blank}}}{A_{\text{control}} - A_{\text{blank}}} \times 100\%$$

where, A was the absorbance of control, blank and sample at 570 nm. The cytotoxicity test was performed in replicates of six wells.

2.8. Statistical analysis

All data were expressed as the mean ± standard deviation (S.D.). Statistical analysis was conducted using paired Students's *t*-test analysis.

3. Results & discussion

3.1. Preparation and characterization of DOX@BSA NPs

The pH-sensitive DOX-loaded BSA NPs were prepared using desolvation technique, followed by crosslinking using glutaraldehyde through Schiff base bonds. The pH-insensitive BSA NPs (iBSA NPs) were also prepared as a negative control. As shown in Figure 2(A), iBSA NPs and sBSA NPs were characterized by dynamic light scattering (DLS), showing that their particle sizes were similar and approximately 120 nm in diameter. After loading DOX, the particle size of DOX_s@BSA NPs slightly increased (c.a. 130 nm) compared with sBSA NPs, resulting from the encapsulation of DOX molecules in the core of NPs through the hydrophobic interaction (Xu et al. 2019). The similar results could be found in Figure 2(B). Furthermore, the narrow distribution curve of BSA-based NPs revealed the low nanoparticle polydispersity and high uniformity, demonstrating that desolvation and crosslink could be useful methods to prepare multi-functional BSA NPs. The TEM image of DOX_s@BSA NPs was showed in supplementary Figure S1. The particle size was approximately 120 nm which was slightly less than that confirmed by DLS. The reason could be due to shrinking of the particles during the drying process prior to TEM analysis. In addition, the DLS data presented an intensity average, which could also be another reason for the discrepancy between DLS and TEM data. Figure 2(C) showed the zeta-potential of iBSA NPs, sBSA NPs and DOX_s@BSA NPs. For the three BSA-based NPs, the zeta-potential was negative, indicating that these BSA-based NPs were able to avoid the interaction with the most proteins with negative charge in biological circulation. In addition, the zeta-potential of DOX_s@BSA NPs was slightly higher

compared with those of iBSA NPs and sBSA NPs, resulting from the loading of positively charged DOX molecules.

To further confirm the optimal DOX formulation, different mass ratios of drug to BSA were performed and studied. The particle size, PDI, LC and EE were shown in Table 1. When the mass ratio was 1: 4 (5 mg of DOX and 20 mg of BSA), the LC and EE were 15.6% and 71.8%, respectively. With increase of mass ratio to 1: 2 (10 mg of DOX and 20 mg of BSA), the LC was obviously increased to 21.4%, while the EE was slightly decreased to 62.0%. When the mass ratios was 1: 1 (20 mg of DOX and 20 mg of BSA), the LC (25.2%) was slightly increased compared with that at mass ratio of 1: 2, but the EE was markedly decreased to 47.9%. In addition, the particle sizes of DOX_s@BSA NPs at different mass ratios were about 130 nm which was slight higher than that of blank sBSA NPs. The PDI was increased after loading of DOX molecules in BSA NPs due to the increased core. The PDI at mass ratio 1: 1 was the highest, possibly resulting from the aggregation of excessive unloaded DOX molecules. Collectively, the formulation at mass ratio of 1: 2 was the optimal, and would be used in the followed studies.

Table 1. Particle size, polydispersity index (PDI), drug loading content (LC) and encapsulation efficacy (EE) of DOX_s@BSA NPs at different mass ratios of drug and BSA carriers.

Carrier (20 mg)	DOX (mg)	LC (%) ^a	EE (%) ^a	Size (nm) ^b	PDI ^b
BSA	0	–	–	120.3	0.138
	5	15.6	71.8	130.1	0.143
	10	21.4	62.0	132.2	0.145
	20	25.2	47.9	135.7	0.156

^aMeasured by UV-vis, ^bmeasured by DLS.

3.2. Ph-sensitivity of DOX_s@BSA NPs

Next, to study the pH-sensitivity of DOX_s@BSA NPs, the particle size and zeta-potential of BSA-based NPs after incubation in PBS with different pH values for 24 h were recorded, as shown in Figure 3(A,B). The particle size of iBSA NPs at pH 7.4 was 121.6 nm. With the decrease of pH, the particle size was dramatically increased (198.1 nm at pH 5.0 and 217.5 nm at pH 3.0) because of swelling of iBSA NPs. For pH-sensitive sBSA NPs, the particle size was firstly increased with decrease of pH values, and the trend was similar to that of iBSA NPs due to the swelling of NPs. In contrast, when the pH was less than 5.0, the particle size of sBSA NPs was decreased to about 15 nm. The reason was that the sBSA NPs were disassembled into BSA, resulting from the cleavage of Schiff base bonds triggered by acidity. The same trend could be observed for DOX_s@BSA NPs at different pH conditions. Figure 3(B) showed the surface charge of iBSA NPs, sBSA NPs and DOX_s@BSA NPs at different pH values. The zeta-potential of three BSA-based NPs was significantly increased with the decrease of pH value. When the pH decreased from 8.0 to 3.0, the surface charge was reversed from negative to positive indicated by the zeta-potential characterization, attributing to the protonation of amine residues in BSA under acidic conditions. Additionally, DOX_s@BSA NPs showed slightly higher zeta-potential in comparison to that of blank BSA NPs, because the amine residues of DOX might also be ionized and enhance the surface charge. In summary, the changes in particle size and surface charge of BSA-based NPs showed that the pH-sensitivity. Then, the NPs system which can be used in biomedical application should have high

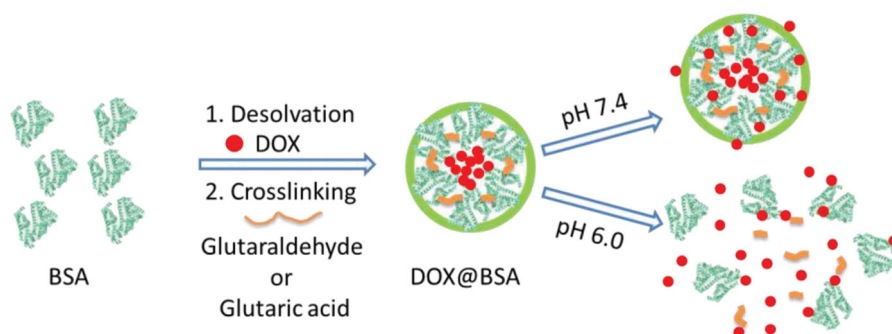


Figure 1. Schematic illustration of fabrication of pH-responsive DOX_s@BSA NPs with pH-triggered drug release profile.

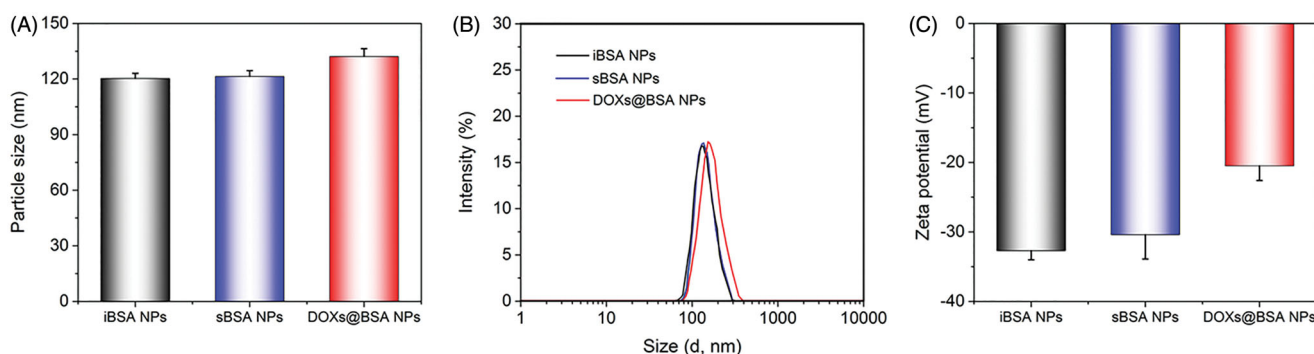


Figure 2. Characterization of BSA-based NPs at pH 7.4 in PBS at room temperature. Particle size (A), distribution (B) and zeta-potential (C) of iBSA NPs, sBSA NPs and DOX_s@BSA NPs measured by DLS ($n = 3$, mean \pm SD).

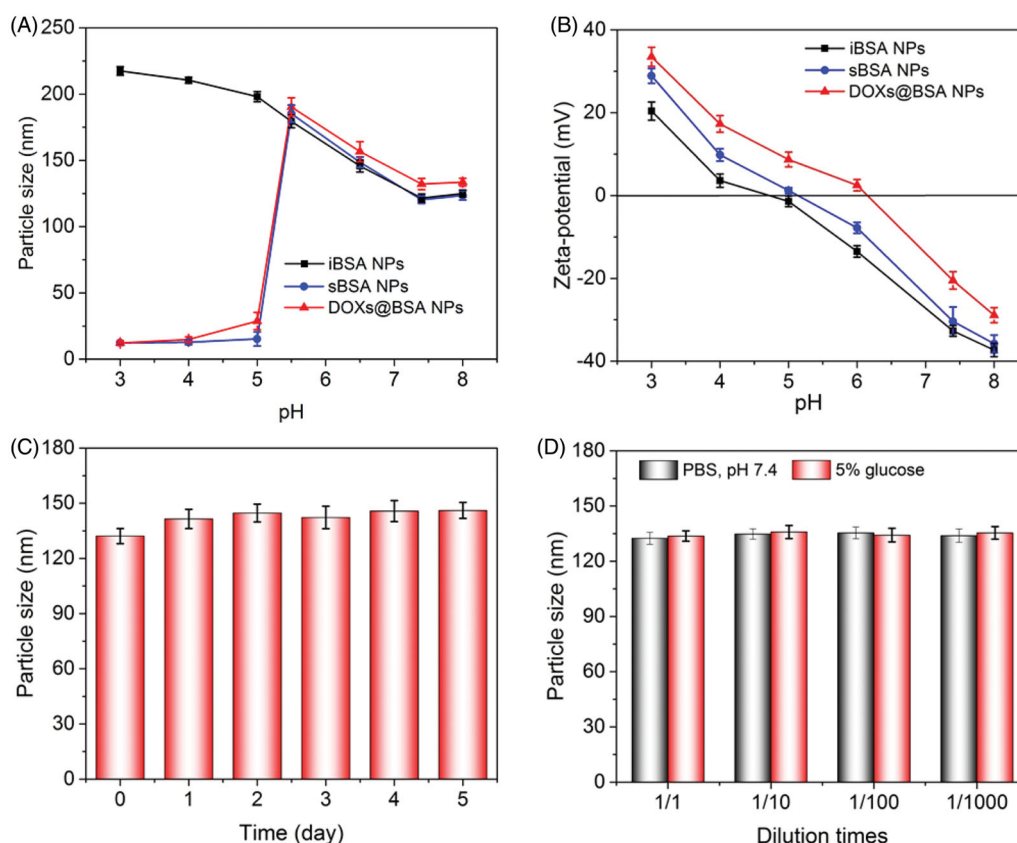


Figure 3. Particle size (A) and zeta-potential (B) of DOX-based NPs incubated in PBS at different pH values for 24 h. (C) Particle size of DOX_s@BSA NPs in PBS at pH 7.4 in the presence of 20% FBS after incubation for 5 days at 37 °C. (D) Particle sizes of the DOX_s@BSA NPs in 5% glucose and PBS, pH 7.4 upon dilution at 1/1, 1/10, 1/100 and 1/1000 of the original concentration of the NPs, which was 2 mg/mL ($n = 3$, mean \pm SD).

stability. Herein, we investigate the serum stability of DOX_s@BSA NPs *in vitro*. The particle size of DOX_s@BSA NPs after incubation in PBS at pH 7.4 with 20% FBS at 37 °C for different time was measured, as shown in Figure 3(C). The particle size of DOX_s@BSA NPs was increased from 132.2 nm to 146.1 nm after incubation for 5 days, but the increasing range was less than 20%, suggesting the high serum stability. The similar results could be found for the zeta-potential changes of DOX_s@BSA NPs (supplementary Figure S2). Moreover, the particle size of DOX_s@BSA NPs in PBS (pH 7.4) or 5% glucose solution after dilution showed no significant changes (Figure 3(D)), indicating the high stability of DOX_s@BSA NPs. These findings demonstrated that the DOX_s@BSA NPs may have prolonged circulation time which is the precondition for drug delivery.

3.3. Dox release profile *in vitro*

Next, to confirm that DOX molecules could be released from DOX_s@BSA NPs dependent on pH, the drug release behavior *in vitro* of DOX_s@BSA NPs was performed in PBS at different pH values at 37 °C. The different pH conditions were selected to simulate the normal physiological condition (7.4) and tumor microenvironment (pH 6.5 and 5.0). The *in vitro* drug release profiles of DOX_s@BSA NPs at pH 7.4, 6.5 and 5.0 were shown in Figure 4. At pH 7.4 and 5.0, the DOX release rate of free DOX was rapid, and the cumulative release amount of DOX was higher than 90% for 12 h at pH 7.4 or 5.0.

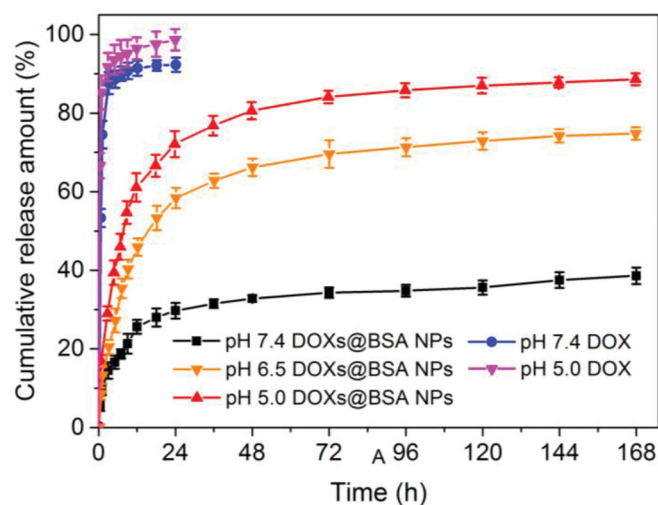


Figure 4. The *in vitro* release profiles of DOX from DOX_s@BSA NPs in different PBS (pH 7.4, 6.5 and 5.0) solutions. The release profiles of free DOX at pH 7.4 and 5.0 were investigated and used as control ($n = 3$, mean \pm SD).

Compared with free DOX, DOX_s@BSA NPs exhibited the sustained drug release behaviors. At pH 7.4, the DOX release rate was slow, and the cumulative release amount of DOX from DOX_s@BSA NPs was only 29.7% and 38.6% for 24 h and 168 h, respectively. In contrast, when the pH decreased to acidic condition, the DOX release rate was obviously accelerated, and the cumulative release amount was higher than 55% (pH 6.5) and 70% (pH 5.0) for 24 h, respectively.

Furthermore, for 148 h, the cumulative release amount was higher than 75% (pH 6.5) and 85% (pH 5.0), respectively. Furthermore, the DOX release rates of DOX-loaded iBSA NPs at pH 7.4 and 5.0 were much lower compared with those of DOX_s@BSA NPs (supplementary Figure S3). These results demonstrated that the acidity can significantly facilitated the drug release rate from DOX_s@BSA NPs, possibly resulting from the disassembly of NPs induced by the pH-triggered cleavage of Schiff base bonds under acidic condition. Furthermore, DOX molecules become more hydrophilic and water-soluble due to the protonation of amine residues in DOX. In summary, the pH-triggered drug release profiles indicated that the DOX_s@BSA NPs might be used for drug delivery and controlled release for cancer chemotherapy.

3.4. Dox release mechanism

We next study the DOX release mechanism of DOX_s@BSA NPs. Although the drug release mechanism of drug-loaded NPs was incompletely understood until now, a comprehensive semi-empirical model has been established to investigate this complex mechanism (Siepmann and Peppas 2012), as follows:

$$\log \left(\frac{M_t}{M_\infty} \right) = n \log t + \log k$$

where, M_t/M_∞ was the cumulative drug release amount at time t . k was a constant which was related to the drug release rate. n was the release exponent which indicated the type of drug release mechanism. When n was about 0.43, the release mechanism corresponded to Fickian diffusion. When n was less than 0.43, the release mechanism might be combination of diffusion and erosion control. When n was higher than 0.43 but lower than 0.85, it could be anomalous transport mechanism. When n was 0.85, the mechanism could be swelling-controlled mechanism.

Basing on this, we further analyzed the DOX release mechanism from DOX_s@BSA NPs at pH 7.4, 6.5 and 5.0. The release process was divided into two stages (0–24 h and 24–168 h), followed by analyzing using the model. Figure 5 showed the theoretical fitted curves based on the experimental data, and the fitting parameters (n and k) at pH 7.4, 6.5 and 5.0 were shown in Table 2. Good linearity could be observed for two stages of drug release profiles at pH 7.4, 6.5 and 5.0 (Figure 5). In the case of pH 7.4, the n value at the first stage was 0.425 (≈ 0.43), indicating that the DOX release mechanism from DOX_s@BSA NPs was Fickian diffusion. The reason could be that the DOX_s@BSA NPs had high stability and maintain compact in PBS at pH 7.4, and the DOX molecules could only diffuse from the NPs. With the increase of time, the n value at the second stage was 0.122 which was much less than 0.43, suggesting that the DOX release mechanism corresponded to combination of diffusion and erosion control because of swelling and erosion of BSA NPs. When the pH decreased to acidic condition, the n value at the first stage was 0.505 (pH 6.5) and 0.538 (pH 5.0) ($0.43 < n < 0.85$) which revealed that the DOX release behavior accorded with the anomalous transport mechanism,

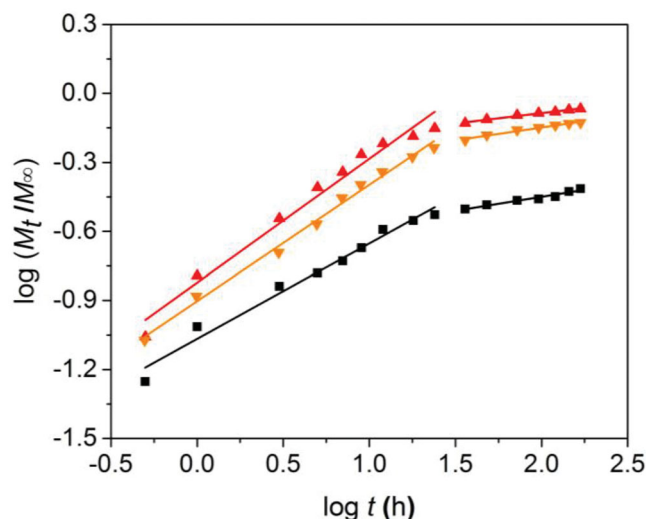


Figure 5. Plots of $\log (M_t/M_\infty)$ against $\log t$ for DOX release from DOX_s@BSA NPs in PBS at pH 7.4, 6.5 or 5.0 at 37 °C.

Table 2. Release exponent (n) and rate constant (k) of DOX from DOX_s@BSA NPs in PBS at pH 7.4, 6.5 or 5.0 at 37 °C.

DOX _s @BSA NPs	pH	n (0–24 h)	k (0–24 h)	n (24–168 h)	k (24–168 h)
DOX	7.4	0.425	0.086	0.122	0.203
	6.5	0.505	0.125	0.111	0.427
	5.0	0.538	0.151	0.090	0.544

resulting from the disassembly of DOX_s@BSA NPs induced by cleavage of Schiff base bonds (Lv et al. 2014). At the second stage, the n values (0.111 for pH 6.5 and 0.090 for 5.0) were much lower than 0.43, demonstrating that the DOX release mechanism was combination of diffusion and erosion control. In addition, the n value at pH 6.5 or 5.0 was much higher than that at pH 7.4, showing that the release rate of DOX was accelerated under acidic condition. Taken together, the pH value played a central role in DOX release from DOX_s@BSA NPs. The release rate and cumulative release amount could be enhanced by the decrease of pH from 7.4 to 5.0, revealing the DOX_s@BSA NPs had pH-triggered drug release profile and might be used for drug delivery and controlled release in biomedical applications.

3.5. Cytotoxicity

Since we have demonstrated that DOX_s@BSA NPs might be used for drug delivery and controlled release, we next evaluated the cytotoxicity against normal cells and tumor cells *in vitro*. MTT assay was performed to study the cytotoxicity of BSA and DOX_s@BSA NPs for NIT 3T3 cells (Figure 6(A)) and tumor cell lines A549 (Figure 6(B)), A2780 (Figure 6(C)) and NCL-H460 (Figure 6(D)), respectively. As shown in Figure 6(A), even at the highest concentration (400 μ g/mL), the cell viability was still higher than 90%. This result displayed that no toxic effect of BSA for NIH 3T3 cells. High cytotoxicity of DOX_s@BSA NPs was observed for the three tumor cell lines. For A549 cells, the cell viability was, respectively, 17.6% and 8.9% for free DOX and DOX_s@BSA NPs at the drug concentration of 20 μ g/mL. And the IC₅₀ values were 1.72 μ g/mL and 0.85 μ g/mL for free DOX and DOX_s@BSA NPs,

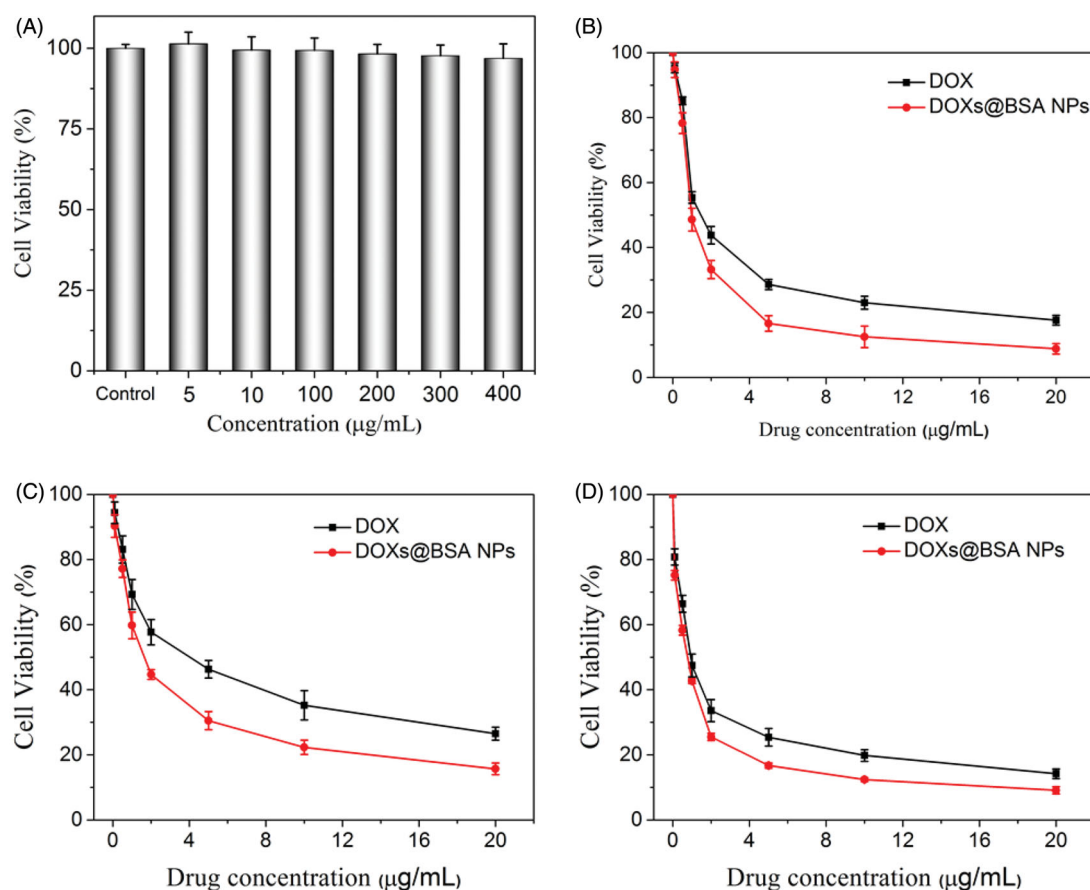


Figure 6. (A) Cell viability of NIH 3T3 cells treated with blank sBSA NPs for 48 h in concentration specified. Cell viability of A549 (B), A2780 (C), and NCL-H460 (D) cells treated with free DOX and DOXs@BSA NPs for 48 h in concentration specified ($n = 6$, mean \pm SD).

respectively. For A2780 cells, IC₅₀ values for free DOX and DOXs@BSA NPs were 4.90 μg/mL and 1.87 μg/mL, respectively, and the DOXs@BSA NPs showed much higher toxic effect against A2780 cells compared with free DOX. For NCL-H460 cells, the cell viability was 14.2% and 9.3% for free DOX and DOXs@BSA NPs at the highest drug concentration, respectively. The IC₅₀ values for free DOX and DOXs@BSA NPs were 0.97 μg/mL and 0.65 μg/mL, respectively. These results demonstrated that the DOXs@BSA NPs exhibited much higher cytotoxicity for tumor cells in comparison to free DOX formulation. The reason might be that the tumor cells could show multidrug resistance for free DOX through the P-gp pumping effect (Alakhov et al. 1999; Qiu et al. 2014). However, the DOXs@BSA NPs could be internalized *via* endocytosis by the tumor cells, and then escaped from the endo/lysosomes, followed by releasing the DOX molecules to induce the apoptosis of tumor cells (Zhang et al. 2009; Oh and Park 2014). Therefore, the DOXs@BSA NPs could inhibit the growth of tumor cells more effectively compared with free DOX. Here, these findings revealed that the DOXs@BSA NPs exhibited much higher cytotoxicity for tumor cells compared with the control free DOX, further indicating the potential application in cancer chemotherapy.

4. Conclusion

In this work, we reported a BSA-based drug delivery system with pH-triggered drug release profile for delivery and

controlled release of DOX. The DOX-loaded BSA NPs was prepared using desolvation method, followed by crosslinking through pH-sensitive Schiff base bonds, resulting in pH-responsive DOX_s@BSA NPs for drug delivery and controlled release (Figure 1). The engineered BSA NPs were able to efficiently load DOX with high drug loading content and encapsulation efficacy (Table 1). The particle size of DOX_s@BSA NPs was about 130 nm, and the surface charge was negative (Figure 2). DOX_s@BSA NPs showed high serum stability and pH-sensitivity, as indicated by size changes and drug release profiles under different conditions (Figures 3 and 4). We further investigated the drug release mechanism under normal physiological condition (pH 7.4) and tumor microenvironment condition (pH 5.0) using semi-empirical equation (Figure 5). Next, we evaluated the toxic effect of BSA for NIH 3T3 cell, and the cytotoxicity of DOX_s@BSA NPs for three tumor cell lines. The results showed that DOX_s@BSA NPs had much higher cytotoxicity compared with free DOX (Figure 6). This study not only reported a pH-responsive nanomedicine which might be used in cancer therapy, but also showed that preparation of stimuli-responsive DDS by engineering the commercial biomaterials could be a promising method to develop multi-functional way.

Disclosure statement

The authors declare no conflict of interest regarding the publication of this paper.

Funding

This work was financially supported by the Liaoning Science and Technology Plan Project [No. 2015010370-301] and Natural Science Foundation of China [No. 81673028].

References

- Agarwal A, Mackey MA, El-Sayed MA, Bellamkonda RV. (2011). Remote triggered release of doxorubicin in tumors by synergistic application of thermosensitive liposomes and gold nanorods. *ACS Nano* 5: 4919–26.
- Alakhov V, Klinski E, Li S, et al. (1999). Block copolymer-based formulation of doxorubicin. From cell screen to clinical trials. *Colloids Surf, B* 16:113–34.
- Baeza A, Colilla M, Vallet-Regí M. (2015). Advances in mesoporous silica nanoparticles for targeted stimuli-responsive drug delivery. *Expert Opin Drug Deliv* 12:319–37.
- Brannon-Peppas L, Blanchette JO. (2004). Nanoparticle and targeted systems for cancer therapy. *Adv Drug Deliv Rev* 56:1649–59.
- Byrne RS, Deasy PB. (2002). Use of commercial porous ceramic particles for sustained drug delivery. *Int J Pharm* 246:61–73.
- Chatterjee K, Zhang J, Honbo N, Karliner JS. (2010). Doxorubicin cardiomyopathy. *Cardiology* 115:155–62.
- Chen Q, Wang C, Cheng L, et al. (2014). Protein modified upconversion nanoparticles for imaging-guided combined photothermal and photodynamic therapy. *Biomaterials* 35:2915–23.
- Chen WH, Liao WC, Sohn YS, et al. (2018). Stimuli-responsive nucleic acid-based polyacrylamide hydrogel-coated metal-organic framework nanoparticles for controlled drug release. *Adv Funct Mater* 28: 1705137.
- Chu D, Gao J, Wang Z. (2015). Neutrophil-mediated delivery of therapeutic nanoparticles across blood vessel barrier for treatment of inflammation and infection. *ACS Nano* 9:11800–11.
- Copur MS. (2019). State of cancer research around the globe. *Oncology (Williston Park, N.Y.)* 33:181–5.
- Datta NR, Rogers S, Bodis S. (2019). Challenges and opportunities to realize “the 2030 agenda for sustainable development” by the United Nations: implications for radiation therapy infrastructure in low- and middle-income countries. *Int J Radiat Oncol Biol Phys* 105:918–33.
- Dickmann P, Emami S, Santhakumar A, et al. (2014). Safe and secure biomaterials. A risk-based alternative approach. London: Chatham House, 1–14.
- Dong X, Sun Z, Wang X, et al. (2017). Simultaneous monitoring of the drug release and antitumor effect of a novel drug delivery system-MWCNTs/DOX/TC. *Drug Deliv* 24:143–51.
- Fakhoury M. (2016). Drug delivery approaches for the treatment of glioblastoma multiforme. *Artif Cells Nanomed Biotechnol* 44:1365–73.
- Feng X, Li D, Han J, et al. (2017). Schiff base bond-linked polysaccharide-doxorubicin conjugate for upregulated cancer therapy. *Mater Sci Eng C Mater Biol Appl* 76:1121–8.
- Ferlay J, Colombet M, Soerjomataram I, et al. (2019). Estimating the global cancer incidence and mortality in 2018: GLOBOCAN sources and methods. *Int J Cancer* 144:1941–53.
- Gong J, Chen M, Zheng Y, et al. (2012). Polymeric micelles drug delivery system in oncology. *J Control Release* 159:312–23.
- Gordon KB, Tajuddin A, Guitart J, et al. (1995). Hand-foot syndrome associated with liposome-encapsulated doxorubicin therapy. *Cancer* 75: 2169–73.
- Guo S, Huang L. (2011). Nanoparticles escaping RES and endosome: challenges for siRNA delivery for cancer therapy. *J Nanomater* 2011:1–12.
- Kong F, Liang Z, Luan D, et al. (2016). A glutathione (GSH)-responsive near-infrared (NIR) theranostic prodrug for cancer therapy and imaging. *Anal Chem* 88:6450–6.
- Lai P-S, Lou P-J, Peng C-L, et al. (2007). Doxorubicin delivery by polyamidoamine dendrimer conjugation and photochemical internalization for cancer therapy. *J Control Release* 122:39–46.
- Larrañeta E, Lutton REM, Woolfson AD, Donnelly RF. (2016). Microneedle arrays as transdermal and intradermal drug delivery systems: materials science, manufacture and commercial development. *Mater Sci Eng R Rep* 104:1–32.
- Li J, Ma YJ, Wang Y, et al. (2018). Dual redox/pH-responsive hybrid polymer-lipid composites: Synthesis, preparation, characterization and application in drug delivery with enhanced therapeutic efficacy. *Chem Eng J* 341:450–61.
- Li S, Shang L, Xu B, et al. (2019). A nanozyme with photo-enhanced dual enzyme-like activities for deep pancreatic cancer therapy. *Angew Chem Int Ed Engl* 58:12624–31.
- Li Y, Xiao K, Zhu W, et al. (2014). Stimuli-responsive cross-linked micelles for on-demand drug delivery against cancers. *Adv Drug Deliv Rev* 66: 58–73.
- Lv S, Tang Z, Zhang D, et al. (2014). Well-defined polymer-drug conjugate engineered with redox and pH-sensitive release mechanism for efficient delivery of paclitaxel. *J Control Release* 194:220–7.
- Makadia HK, Siegel SJ. (2011). Poly lactic-co-glycolic acid (PLGA) as biodegradable controlled drug delivery carrier. *Polymers (Basel)* 3: 1377–97.
- Mariam J, Sivakami S, Dongre PM. (2016). Albumin corona on nanoparticles - a strategic approach in drug delivery. *Drug Deliv* 23:2668–76.
- Masood F. (2016). Polymeric nanoparticles for targeted drug delivery system for cancer therapy. *Mater Sci Eng C Mater Biol Appl* 60:569–78.
- Mellman I, Coukos G, Dranoff G. (2011). Cancer immunotherapy comes of age. *Nature* 480:480–9.
- Min KH, Park K, Kim Y-S, et al. (2008). Hydrophobically modified glycol chitosan nanoparticles-encapsulated camptothecin enhance the drug stability and tumor targeting in cancer therapy. *J Control Release* 127: 208–18.
- Mura S, Nicolas J, Couvreur P. (2013). Stimuli-responsive nanocarriers for drug delivery. *Nat Mater* 12:991–1003.
- Oh KS, Song JY, Cho SH, et al. (2010). Paclitaxel-loaded pluronic nanoparticles formed by a temperature-induced phase transition for cancer therapy. *J Control Release* 148:344–50.
- Oh N, Park J-H. (2014). Endocytosis and exocytosis of nanoparticles in mammalian cells. *Int J Nanomed* 9:51–63.
- Peng X, Liu P, Pang B, et al. (2019). Facile fabrication of pH-responsive nanoparticles from cellulose derivatives via Schiff base formation for controlled release. *Carbohydr Polym* 216:113–8.
- Qiao Y, Wan J, Zhou L, et al. (2019). Stimuli-responsive nanotherapeutics for precision drug delivery and cancer therapy. *Wiley Interdiscip Rev Nanomed Nanobiotechnol* 11:e1527.
- Qiu L, Qiao M, Chen Q, et al. (2014). Enhanced effect of pH-sensitive mixed copolymer micelles for overcoming multidrug resistance of doxorubicin. *Biomaterials* 35:9877–87.
- Riley RS, June CH, Langer R, Mitchell MJ. (2019). Delivery technologies for cancer immunotherapy. *Nat Rev Drug Discov* 18:175–96.
- Saha A, Pradhan N, Chatterjee S, et al. (2019). Fatty-amine-conjugated cationic bovine serum albumin nanoparticles for target-specific hydrophobic drug delivery. *ACS Appl Nano Mater* 2:3671–83.
- Saini P, Arora M, Kumar MR. (2016). Poly(lactic acid) blends in biomedical applications. *Adv Drug Deliv Rev* 107:47–59.
- Sandhu PS, Beg S, Mehta F, et al. (2015). Novel dietary lipid-based self-nanoemulsifying drug delivery systems of paclitaxel with p-gp inhibitor: implications on cytotoxicity and biopharmaceutical performance. *Exp Opin Drug Deliv* 12:1809–22.
- Sharma BK. (2017). Synthetic and natural compounds as anti-cancer agents-a review. *Asia J Res Chem* 10:699–707.
- Siepmann J, Peppas NA. (2012). Modeling of drug release from delivery systems based on hydroxypropyl methylcellulose (HPMC). *Adv Drug Delivery Rev* 64:163–74.
- Singal PK, Iliskovic N. (1998). Doxorubicin-induced cardiomyopathy. *N Engl J Med* 339:900–5.
- Soma CE, Dubernet C, Barratt G, et al. (2000). Investigation of the role of macrophages on the cytotoxicity of doxorubicin and doxorubicin-loaded nanoparticles on M5076 cells in vitro. *J Control Release* 68: 283–9.

- Sun J, Zhang L, Zhang Y, et al. (2019). Smart albumin-loaded Rose Bengal and doxorubicin nanoparticles for breast cancer therapy. *J Microencapsul* 36:728–37.
- Sun T, Zhang YS, Pang B, et al. (2014). Engineered nanoparticles for drug delivery in cancer therapy. *Angew Chem Int Ed Engl* 53:12320–64.
- Wang Y, Yan J, Wen N, et al. (2020). Metal-organic frameworks for stimuli-responsive drug delivery. *Biomaterials* 230:119619.
- Wei Y, Gao L, Wang L, et al. (2017). Polydopamine and peptide decorated doxorubicin-loaded mesoporous silica nanoparticles as a targeted drug delivery system for bladder cancer therapy. *Drug Deliv* 24: 681–91.
- Xu H, Dong L, Bin Z, et al. (2020). Supramolecular self-assembly of a hybrid 'hyalurosomes' for targeted photothermal therapy in non-small cell lung cancer. *Drug Deliv* 27:378–86.
- Xu M, Zhang CY, Wu J, et al. (2019). PEG-detachable polymeric micelles self-assembled from amphiphilic copolymers for tumor-acidity-triggered drug delivery and controlled release. *ACS Appl Mater Interfaces* 11:5701–13.
- Yang ST, Liu Y, Wang YW, Cao A. (2013). Biosafety and bioapplication of nanomaterials by designing protein-nanoparticle interactions. *Small* 9: 1635–53.
- Yin Q, Shen J, Zhang Z, et al. (2013). Reversal of multidrug resistance by stimuli-responsive drug delivery systems for therapy of tumor. *Adv Drug Deliv Rev* 65:1699–715.
- Zeng D, Wang L, Tian L, et al. (2019). Synergistic photothermal/photodynamic suppression of prostatic carcinoma by targeted biodegradable MnO₂ nanosheets. *Drug Deliv* 26:661–72.
- Zhang CY, Peng S, Zhao B, et al. (2017). Polymeric micelles self-assembled from amphiphilic polymers with twin disulfides used as siRNA carriers to enhance the transfection. *Mater Sci Eng C* 78: 546–52.
- Zhang CY, Yang YQ, Huang TX, et al. (2012). Self-assembled pH-responsive MPEG-b-(PLA-co-PAE) block copolymer micelles for anticancer drug delivery. *Biomaterials* 33:6273–83.
- Zhang S, Li J, Lykotrafitis G, et al. (2009). Size-dependent endocytosis of nanoparticles. *Adv Mater Weinheim* 21:419–24.
- Zhang X, Zhang C, Cheng M, et al. (2019). Dual pH-responsive "charge-reversal like" gold nanoparticles to enhance tumor retention for chemo-radiotherapy. *Nano Res* 12:2815–26.
- Zhou X, Guo L, Shi D, et al. (2020). Ultrasound-responsive highly biocompatible nanodroplets loaded with doxorubicin for tumor imaging and treatment in vivo. *Drug Deliv* 27:469–81.